Results of a search for the $h_c(^1P_1)$ state of charmonium in the $\eta_c\gamma$ and $J/\psi\pi^0$ decay modes

M. Andreotti,[2] S. Bagnasco,[3,7] W. Baldini,[2] D. Bettoni,[2] G. Borreani,[7] A. Buzzo,[3] R. Calabrese,[2] R. Cester,[7] G. Cibinetto,[2] P. Dalpiaz,[2] G. Garzoglio,[1] K. E. Gollwitzer,[1] M. Graham,[5] M. Hu,[1] D. Joffe,[6] J. Kasper,[6] G. Lasio,[7,4] M. Lo Vetere,[3] E. Luppi,[2] M. Macrì,[3] M. Mandelkern,[4] F. Marchetto,[7] M. Marinelli,[3] E. Menichetti,[7] Z. Metreveli,[6] R. Mussa,[2,7] M. Negrini,[2] M. M. Obertino,[7,5] M. Pallavicini,[3] N. Pastrone,[7] C. Patrignani,[3] T. K. Pedlar,[6] S. Pordes,[1] E. Robutti,[3] W. Roethel,[6,4] J. L. Rosen,[6] P. Rumerio,[7,6] R. Rusack,[5] A. Santroni,[3] J. Schultz,[4] S. H. Seo,[5] K. K. Seth,[6] G. Stancari,[1,2] M. Stancari,[4,2] A. Tomaradze,[6] I. Uman,[6] T. Vidnovic III,[5] S. Werkema,[1] and P. Zweber[6]

(Fermilab E835 Collaboration)

[1]*Fermi National Accelerator Laboratory, Batavia, Illinois 60510, USA*
[2]*Istituto Nazionale di Fisica Nucleare and University of Ferrara, 44100 Ferrara, Italy*
[3]*Istituto Nazionale di Fisica Nucleare and University of Genova, 16146 Genova, Italy*
[4]*University of California at Irvine, California 92697, USA*
[5]*University of Minnesota, Minneapolis, Minnesota 55455, USA*
[6]*Northwestern University, Evanston, Illinois, 60208, USA*
[7]*Istituto Nazionale di Fisica Nucleare and University of Torino, 10125, Torino, Italy*
(Received 13 May 2005; published 4 August 2005)

We report evidence for the h_c state of charmonium in its $\eta_c\gamma$ decay mode and lack of evidence in the $J/\psi\pi^0$ mode. We studied these channels in $\overline{p}p$ annihilations near the center of gravity of the ^3P_J states, where the h_c was reported in the $J/\psi\pi^0$ mode by E760, our previous experiment, at $3526.2 \pm 0.15 \pm 0.2$ MeV, with $\Gamma_R \leq 1$ MeV. We observe an event excess in the $\eta_c\gamma$ mode near 3526 MeV. Testing the null hypothesis of a linearly varying background cross section against the alternate hypothesis that includes a resonance near 3526 MeV, we reject the null hypothesis with $\mathcal{P} \sim 0.001$. The resonance mass is $3525.8 \pm 0.2 \pm 0.2$ MeV and the resonance width ≤ 1 MeV. We estimate $10.0 \pm 3.5 < \Gamma_{\overline{p}p}\mathcal{B}_{\eta_c\gamma} < 12.0 \pm 4.5$ eV, corresponding to fixed values $0.5 < \Gamma_R < 1.0$ MeV. We find no event excess within the search region in the $J/\psi\pi^0$ mode.

DOI: 10.1103/PhysRevD.72.032001 PACS numbers: 13.75.Cs, 14.40.Gx

I. INTRODUCTION

Heavy quarkonium physics continues to be an important field for our understanding of QCD [1]. Charmonium occupies an intermediate regime between the $\bar{b}b$ system, where an expansion in the strong coupling constant is justifiable, and the light mesons, where nonperturbative effects dominate. Of the charmonia below the $\bar{D}D$ threshold, the $h_c(1^1P_1(1^{+-}))$ is the least accessible. The $^3S_1$ states (J/ψ and ψ') are formed in e^+e^- annihilations, and the ^3P and ^1S states are populated, respectively, by $E1$ and $M1$ decays of the $^3S_1$ states. In e^+e^- annihilations, either sequential radiative transitions through the χ_{c2} (E1 followed by M1), or an I-spin-forbidden pionic transition from the ψ' can potentially populate the h_c state. The observation of the h_c, resonantly formed in $\overline{p}p$ annihilations, is one of the principal objectives of experiments E760 and E835 at Fermilab. In 1992, E760 reported the observation of the h_c in the $J/\psi\pi^0$ decay mode, at $E_R = 3526.2 \pm 0.15(\text{stat}) \pm 0.2(\text{syst})$ MeV with $\Gamma_R \leq 1.1$ MeV (90% confidence level) [2]. We estimated the probability that such an observation could arise by chance in our search region as $1/400$.

We subsequently made two additional data runs as E835 with the upgraded detector described in Ref. [3]. In both of these we took data in the h_c search region and in several nearby regions that are suitable for background determination. In this article we describe the analysis of the possible $J/\psi\pi^0$ and $\eta_c\gamma$ decay modes of the h_c using the data for both runs.

The observation of the h_c is important because a comparison of its mass with the masses of the $3P$ states provides information on the spin dependence of the $\bar{Q}Q$ interaction. In the QCD potential model [4], the confining potential makes no contribution to the hyperfine interaction and the Coulombic one-gluon potential leads to a hyperfine splitting only in S states. Thus the hyperfine splitting in the P states, given by the difference between the spin-weighted average mass of the $3P$ states $\langle M(^3P_J)\rangle$ and that of the h_c, is predicted to be close to zero. The corrections to this result are small and nearly all theoretical papers [5] predict this splitting to be several MeV or less. The current experimental value of $\langle(^3P_J)\rangle$ is 3525.30 ± 0.07 MeV [6], permitting determination of the hyperfine splitting if the h_c mass can be accurately measured.

In $\overline{p}p$ annihilations, charmonium states are formed by the coherent annihilations of the three quarks of the proton and the three antiquarks of the antiproton. The h_c is expected to be less than 1 MeV in width and to decay with

roughly equal rates by the $E1$ transition to $\eta_c\gamma$ and to light hadrons [7].

II. EXPERIMENTAL TECHNIQUE

The E835 experiment has been described in detail elsewhere [3]. In brief, antiprotons are stored and stochastically cooled in the Fermilab Antiproton Source until the desired number, a *stack* of typically $\sim 6 \times 10^{11}$, has been accumulated. The $\bar{p}$ are then decelerated until the desired energy is reached. The internal hydrogen-gas-jet target is turned on and data taking is begun. Within a stack, data are taken at different energies, identified as *runs*, by accelerating or decelerating the stored beam. The reaction products are identified in the nonmagnetic detector, which is optimized for the detection of photons and $e^{\pm}$. The detector is cylindrical, consisting of three scintillator hodoscopes H1, H2′, and H2, followed by a multicell threshold Čerenkov detector and a 1280-element lead-glass electromagnetic calorimeter (CCAL). Two cylindrical chambers built of proportional drift tubes and a scintillating fiber tracking chamber were used for charged-particle tracking in 1997. An additional fiber tracker was added for the year-2000 run. A plane of scintillation counters (FCH) and a planar lead-glass calorimeter (FCAL) are used to detect forward-going particles. The luminosity monitor counts small-angle elastic scatters.

With respect to E760, the most important detector modifications were:

(1) We implemented pulse shaping and added a time-to-digital converter for each channel of the CCAL and FCAL in order to manage pileup and accidentals at higher instantaneous luminosities.
(2) We replaced the E760 FCAL with an array of lead-glass modules [3]. In E835-1997 this detector was operational for $\approx 50\%$ of the time. In E835-2000 it was 100% operational.

We investigate the following reactions:

$$\bar{p}p \to h_c \to J/\psi\pi^0, \qquad J/\psi \to e^+e^-, \qquad \pi^0 \to \gamma\gamma, \tag{1}$$

$$\bar{p}p \to h_c \to \eta_c\gamma, \qquad \eta_c \to \gamma\gamma. \tag{2}$$

Tables I and II give the range of center-of-mass (cm) energies $\sqrt{s}$, the rms cm-energy widths $\sigma(\sqrt{s}) \sim$ 0.2–0.5 MeV, the integrated luminosities L, and the candidate totals for each stack. In the analysis, each run, with a typical integrated luminosity of 0.2 pb^{-1}, is considered separately.

TABLE I. E835-1997 data sample analyzed: the range of cm energies, mean rms width, integrated luminosity L, and candidate totals for each stack. In the analysis, each run, with a typical integrated luminosity of 0.2 pb^{-1}, is considered separately.

Stack	$\sqrt{s}$ MeV	$\sigma_{\sqrt{s}}$ keV	L pb^{-1}	Candidates $\eta_c\gamma$	$J/\psi\pi^0$
I-χ_{c_1} scans	3470–3515	···	5.82	0	
I-61	3524.50–3524.68	304	3.72	0	9
I-58	3525.06–3525.22	280	2.90	0	10
I-62	3525.35–3525.58	282	3.53	0	10
I-55	3525.49–3525.76	292	3.48	1	15
I-60	3525.70–3525.86	282	2.98	1	9
I-63	3525.77–3525.86	281	3.82	3	2
I-59	3525.79–3525.89	244	1.20	0	2
I-19	3526.08–3526.11	411	1.99	2	3
I-56	3526.05–3526.14	295	2.29	0	3
I-57	3526.10–3526.32	295	3.31	0	6
I-51	3526.47–3526.55	317	0.98	0	2
I-64	3526.50–3526.55	282	3.23	1	7
I-54	3526.51–3526.51	296	0.65	0	0
I-52	3526.70–3526.94	256	3.09	0	7
I-53	3527.39–3527.55	215	1.40	0	1
I-50	3529.04–3529.19	402	2.33	0	6
I-15	3534.21–3535.67	533	1.30	0	3
I-χ_{c_2}	3545–3565	···	11.10	1	
I-η_c'search	3570–3670	···	33.99	2	
I-ψ'	3670–3695	···	9.00	0	
I-high energy	3700–4400	···	2.61	0	

TABLE II. E835-2000 data sample analyzed: the range of cm energies, mean rms width, integrated luminosity L, and candidate totals for each stack. In the analysis, each run, with a typical integrated luminosity of 0.2 pb^{-1}, is considered separately.

Stack	$\sqrt{s}$ MeV	$\sigma_{\sqrt{s}}$ keV	L pb^{-1}	Candidates $\eta_c\gamma$	$J/\psi\pi^0$
II-χ_{c0} scans	3330–3400	···	8.51	2	
II-χ_{c0} scans	3400–3430	···	24.35	3	
II-χ_{c1} scans	3470–3515	···	5.98	0	
II-23	3523.27–3523.43	390	3.06	0	8
II-39	3524.78–3524.80	297	2.03	0	3
II-21	3525.16–3525.18	300	3.51	0	5
II-20	3525.46–3525.50	309	4.31	1	13
II-16	3525.70–3525.75	376	3.32	1	10
II-37	3525.87–3525.89	256	1.67	1	4
II-38	3525.88–3525.91	288	1.64	1	8
II-18	3526.01–3526.06	294	3.74	3	9
II-15	3526.14–3526.25	442	3.67	0	3
II-24	3526.18–3526.34	346	0.51	0	1
II-36	3526.27–3526.29	268	1.65	0	8
II-35	3526.26–3526.31	291	1.49	0	5
II-41	3526.29–3526.33	253	1.95	0	8
II-22	3526.24–3526.30	280	2.63	0	11
II-25	3526.30–3526.33	304	0.95	0	2
II-26	3526.40–3526.46	328	2.47	0	5
II-17	3526.51–3526.59	291	3.71	0	8
II-19	3526.86–3526.90	311	3.04	0	8
II-40	3527.29	265	1.22	0	2
II-28	3528.61–3528.62	364	1.28	0	3
II-27	3529.09–3529.13	385	2.47	0	6
II-χ_{c2}	3545–3565	···	1.12	0	
II-ψ'	3670–3695	···	14.51	0	
II-high energy	3700–4400	···	7.26	0	

didate totals for the $\eta_c\gamma$ and $J/\psi\pi^0$ reactions. The cm energy for each event is obtained from an off-line calculation that relies upon the contemporaneous measurement of the beam-revolution frequency and beam-orbit length of the stored antiproton beam. We estimate the (rms) experimental uncertainty in the central energy to be 0.07 MeV. The uncertainty in the absolute center-of-mass energy is ± 0.02 MeV due to uncertainty in the ψ' mass, which is used to determine the reference beam-orbit length. During part of the E835-1997 data taking, some of the beam-position monitors, used to determine the beam-orbit length, were miscalibrated. The cm energies for these data have reduced precision.

The geometrical and cut efficiencies are calculated using the detector simulation, and include the effects of dead calorimeter channels as well as stack-by-stack variations in the calibration. The effect of extraneous interactions overlapping signal events is included by overlaying events from randomly timed triggers onto a set of simulated events. Efficiencies are calculated for each energy point in order to take into account the different run conditions. The method of using the detector simulation to calculate efficiencies was checked previously [3] for $e^+e^-\gamma$ events and other data samples.

A. $\eta_c\gamma$ Reaction

1. Trigger and Event Selection

We used a two-branch trigger system to record neutral events having either two large back-to-back energy deposits **PBG3**, or at least 80% of the total available energy deposited in the CCAL **ETOT-HI** [3]. For neutral triggers, the charged-particle veto was the *OR* of a coincidence between corresponding counters of the two innermost scintillator hodoscopes, H1 and H2′, and the forward scintillator hodoscope FCH.

In the off-line selection, we reject events with H2′ or H2 signals not in coincidence with the corresponding Čerenkov counter. Those with coincidences are retained as events in which a photon converted after H1. We select events containing three *candidate* photons in CCAL, defined as clusters with energy >20 MeV (>5 MeV in the central block) occurring within 6 ns of the trigger time. We reject those with an FCAL signal within 6 ns of the trigger time. We define an *undetermined* cluster as one without timing information, or with $E_{\rm cluster} < 300$ MeV and occurring within 15 ns of the trigger. We reject events where the invariant mass of a candidate photon with any other candidate or undetermined cluster satisfies $|m_{\gamma\gamma} - m_{\pi^0}| < 35$ MeV. We determine the acceptance for the selection to be $\sim 26\%$ by simulation, using the known differential cross section for this reaction: electric-dipole decay of the h_c followed by the isotropic decay of the η_c.

The main background to single-photon showers is showers produced by coalesced π^0 decays. We develop a likelihood ratio, which we call the photon weight (*PW*), to discriminate between these alternatives. This measure is analogous to the electron weight (*EW*) described in Ref. [3], where the variables given below are described. It is based on the following attributes of the shower:

(1) s_θ and s_ϕ, the cluster second moments.
(2) cluster mass, given by

$$M_{cl} = \sqrt{\left(\sum_i E_i\right)^2 - \left(\sum_i \mathbf{p}_i\right)^2} \qquad (3)$$

obtained from the calorimeter block energies for a 5×5 matrix centered on the shower.
(3) F_{35}, the ratio of the energy in a 3×3 matrix to that in a 5×5 block matrix centered on the shower.
(4) F_{24}, the ratio of the energy in a 2×2 matrix to that in a 4×4 matrix centered on the shower.

We use a clean set of χ_{c1} and χ_{c2} events ($\chi_{cJ} \to J/\psi\gamma \to e^+e^-\gamma$), where the energies are comparable to those of h_c radiative decay, as a source of single-photon showers for the probability density functions used in the likelihood ratio, the γ for the lowest-energy photon, and the e^+e^- for the higher-energy photons. We use candidates for $\bar{p}p \to e^+e^-\gamma$, with $M_{e^+e^-} < 2800$ MeV, taken in the χ_{c1} and χ_{c2} regions, as a source of events enriched in showers produced by coalesced π^0 decays. Figure 1 shows

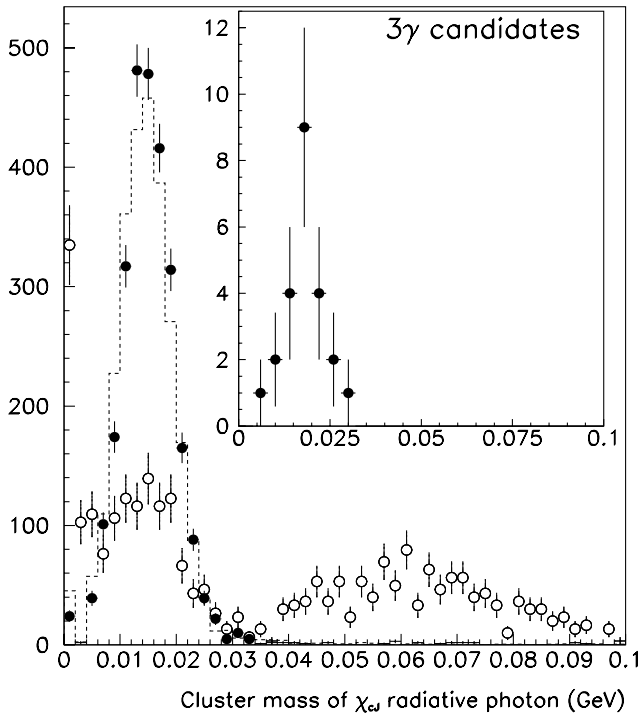

FIG. 1. The cluster-mass distribution of the photon for a clean sample of $\chi_{cJ} \to J/\psi\gamma \to e^+e^-\gamma (J = 1, 2)$ events (solid) and for candidates for the process $\bar{p}p \to e^+e^-\gamma$, with $M_{e^+e^-} < 2800$ MeV (open). The latter data set is enriched in coalesced π^0 showers. The inset shows the lowest-energy photon for the $h_c \to \eta_c\gamma \to 3\gamma$ candidates. The dashed histogram is the prediction of the simulation.

the cluster-mass distribution for the lowest-energy photon and Fig. 2 for the higher-energy photons for our candidates. In both plots we also show corresponding distributions for the clean χ_{cJ} events and candidate $e^+e^-\gamma$ events with $M_{e^+e^-} < 2800$ MeV. The distributions for our candidates are compatible with the corresponding ones for the clean $e^+e^-\gamma$ events; the lowest-energy and higher-energy photons are distinctly separated, and the sample of $e^+e^-\gamma$ candidates enriched in coalesced π^0 showers contains many showers with *bad* cluster masses. We cut on PW, the ratio of likelihoods for the photon and background shower hypotheses, so that $PW_1 \times PW_2 > 1$ and $PW_3 > 1.5$, where the γs are ordered so that $E_{\gamma 1} > E_{\gamma 2} > E_{\gamma 3}$, where the E_γ are cm energies.

A four-constraint kinematical fit to the hypothesis $\overline{p}p \to 3\gamma$ is performed and we require a nominal χ^2 probability $\mathrm{P}(3\gamma) > 10^{-4}$. If there are undetermined clusters in the event, we require that $\mathrm{P}(3\gamma) > \mathrm{P}(4\gamma)$, the latter being the nominal χ^2 probability for any fit to $\overline{p}p \to 4\gamma$. (These cuts do not remove any events that would not be removed by the subsequent cut on the fit probability for $\overline{p}p \to \eta_c\gamma$. However we discuss them to demonstrate their relatively high efficiencies.) By simulation we determine that these cuts reduce the acceptance $\times$ efficiency product to $\sim$18.5%.

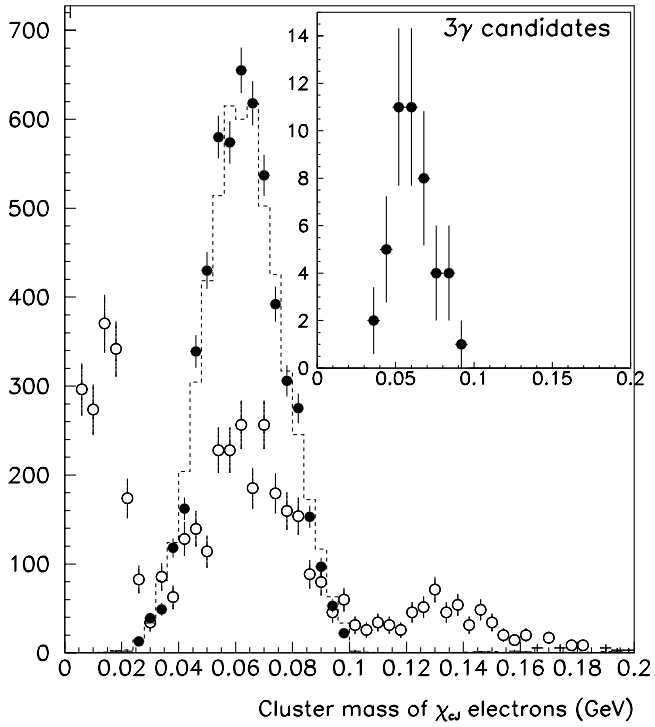

FIG. 2. The cluster-mass distribution of the electrons for a clean sample of $\chi_{cJ} \to J/\psi\gamma \to e^+e^-\gamma (J = 1, 2)$ events (solid) and for candidates for the process $\bar{p}p \to e^+e^-\gamma$, with $M_{e^+e^-} <$ 2800 MeV (open). The latter data set is enriched in coalesced π^0 showers (open). The inset shows the higher-energy photons for the $h_c \to \eta_c\gamma \to 3\gamma$ candidates. The dashed histogram is the prediction of the simulation.

The Dalitz plot for the candidate events in the h_c band, selected to be $3524 < \sqrt{s} < 3524$ MeV, is given in Fig. 3, where we plot measured quantities. For $\overline{p}p \to \eta_c\gamma$ at 3526 MeV, the η_c band follows a straight line connecting points at 3.553 GeV^2 on the M_{13}^2 and M_{23}^2 axes. No π^0 band is seen due to the cut on $m_{\gamma\gamma}$ described above. We observe η and η' bands as well as a continuum of events for $M_{13}^2 >$ 1 GeV^2, $M_{23}^2 > 1$ GeV^2. These features are derived, respectively, from $\overline{p}p \to \pi^0\eta$, $\pi^0\eta'$, and $3\pi^0$ events, where the π^0s decay symmetrically or highly asymmetrically; for such a π^0 decay only a single cluster, in approximately the direction of the π^0, is identified. We refer to events where a π^0 is misidentified as a γ as *feed-down* events.

Symmetrical π^0 decays, where the 2 photon showers coalesce to produce a single calorimeter cluster, and highly asymmetrical π^0 decays, where the lower-energy photon is undetected, both contribute to background. The discrimination of our selection depends upon the π^0 energy. For lower-energy π^0s, the photon weight PW, which includes the cluster mass shown in Fig. 1, is highly effective at discriminating against coalesced π^0 decays but the overall fit is relatively ineffective at eliminating events with highly asymmetrical π^0 decays. For higher-energy π^0s, PW is less effective at discriminating against coalesced π^0 decays as shown in Fig. 2, but the overall fit is more effective at eliminating events with highly asymmetrical π^0 decays.

An informative process, as seen from the proximity of some of the corresponding events to our signal events in the

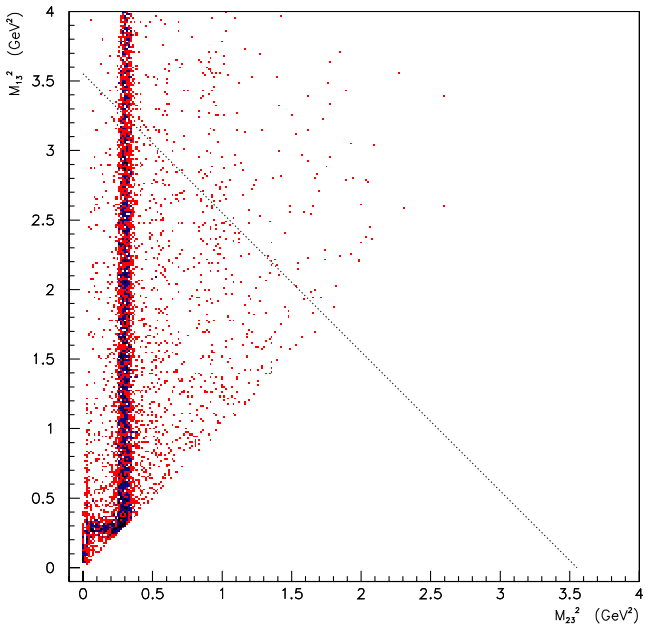

FIG. 3 (color online). Dalitz plot for events fitting $\overline{p}p \to \gamma\gamma\gamma$ for $3524 < \sqrt{s} < 3527$ MeV. A cut has been made which removes events containing π^0s. The dotted line indicates the center of the expected η_c band.

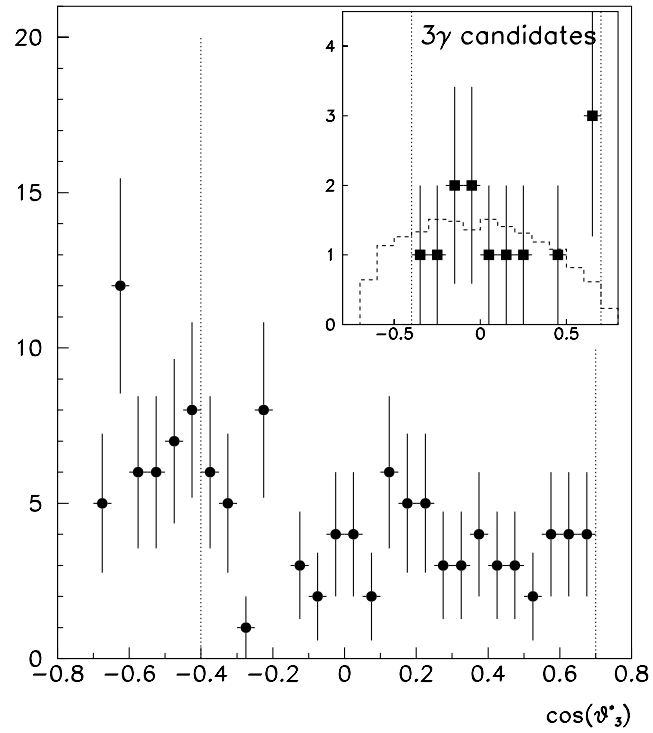

FIG. 4. Center-of-mass angular distribution of γ_3 showing a backward peak due to feed-down events. Cuts have been made that remove events containing π^0s and those with $|\cos\theta_1^*| < 0.5$ or $|\cos\theta_2^*| < 0.5$. The inset shows the h_c candidates between 3525.6 and 3526.4 MeV. The dashed histogram is the corresponding distribution obtained from the simulation. The dotted lines represent the cut made on $\cos\theta_3^*$.

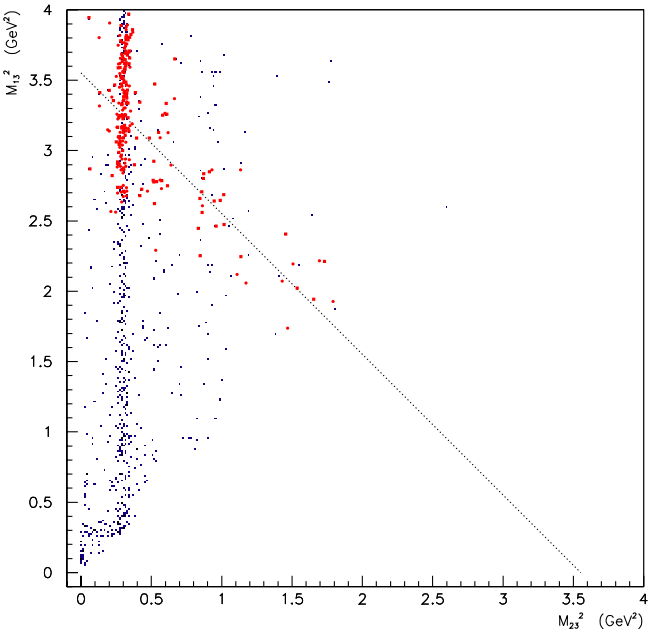

FIG. 5 (color online). Dalitz plot for events fitting $\overline{p}p \to \gamma\gamma\gamma$ (small dots) for $3524 < \sqrt{s} < 3527$ MeV and those fitting $\overline{p}p \to \eta_c\gamma \to \gamma\gamma\gamma$ (large dots). Cuts 1 and 2 on γ cm angles described in the text have been made. The dotted line indicates the center of the expected η_c band.

Dalitz plot, is the formation of $\eta'\pi^0$, followed by $\eta' \to \gamma\gamma$ decay. We recently measured the cross section for $\eta'\pi^0$ formation at a nearby energy [8] and can thus estimate, from the data, the feed-down to the 3γ reaction. In this reaction we discriminate against the decay of (on average) a reasonably energetic π^0, with energy between the higher-energy photons from η_c decay and the lower-energy recoil photon from $h_c \to \eta_c\gamma$.

The integrated cross section for $\eta'\pi^0$ within our acceptance ($-0.6 < \cos\theta_{\rm cm} < 0.6$) is approximately 50 nb. The integrated luminosity for $3524 < \sqrt{s} < 3527$ is $\sim$80 pb^{-1} yielding $\sim$80 000 events, where $BR(\eta' \to 2\gamma) \sim 0.02$. The η' band in Fig. 5 contains $\sim$50 events for a suppression factor of $\sim$0.0006, which comes both from the PW selection, which mainly suppresses the coalesced decays of π^0, and from the kinematical fit, which mainly suppresses events with highly asymmetrical π^0 decays.

For $3\pi^0$ events to be misidentified as 3γ events, three unrecognized coalesced or asymmetrical decays must be present. The suppression factor is expected to be much larger than that for the $\eta'\pi^0$ reaction, accounting for the small background.

We make a sequence of cuts to further reduce the background.

(1) Since the $\bar{p}p$ annihilations to two and three light mesons are strongly forward/backward peaked, the angular distribution for feed-down events is forward/backward peaked. As the cm angular distribution of γ_1 and γ_2 from $\eta_c\gamma$ is nearly uniform, we require that $|\cos\theta_1^*| < 0.5$, $|\cos\theta_2^*| < 0.5$, reducing the acceptance$\times$ efficiency to $\sim$13.5%.

(2) The cm angular distribution for the radiative decay of the $h_c \to \eta_c\gamma$ is $(dN)/(d\cos\theta_3^*) \propto \sin^2\theta_3^*$, while the data show a backward peak, as seen in Fig. 4. The reactions $\overline{p}p \to \pi^0 X^0$ are forward-backward symmetric in the cm frame. However, forward π^0 are more likely to be misidentified as single photons, producing feed-down events where relatively low-energy photons go backward. We thus require that $-0.4 < \cos\theta_3^* < 0.7$, which reduces the acceptance$\times$ efficiency to $\sim$10.9%.

(3) We apply a two-vertex, 5C kinematical fit to $\eta_c\gamma$ and set a χ^2 probability cut at $>$0.01, which we find by simulation reduces the overall acceptance$\times$ efficiency to $\sim$8.5%. The events in the h_c band $3524 < \sqrt{s} < 3527$ MeV selected by the cm angular cuts (small dots) and those also fitting $\eta_c\gamma$ (large dots) are shown in Fig. 5. The dotted line shows the center of the $\eta_c\gamma$ band, in which we expect a uniform density of signal events. Although we have a large number of $\eta_c\gamma$ fits from the $\pi^0\eta$ and $\pi^0\eta'$ channels, for $M_{23} > 1000$ MeV we have a group of events compatible with the reaction $\overline{p}p \to \eta_c\gamma$

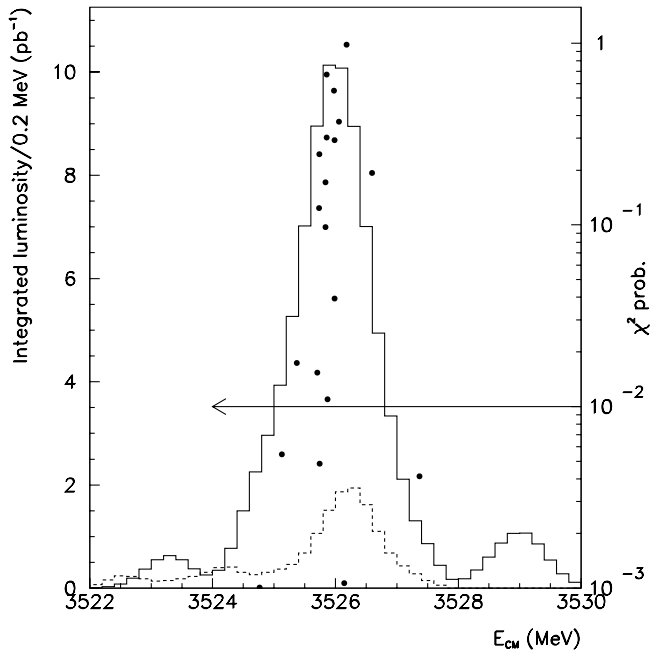

FIG. 6. χ^2 probability vs $\sqrt{s}$ for $\overline{p}p \to \eta_c\gamma$ candidates with cm energies from 3522 to 3530 MeV, where the horizontal line represents the cut used in this analysis. The integrated luminosities for E835 and E760 are shown, respectively, as undashed and dashed histograms.

with relatively little background. In Fig. 6 we plot the χ^2 probability against $\sqrt{s}$ for 5C kinematical fits to $\eta_c\gamma$ for candidates with $3522 < \sqrt{s} < 3530$ MeV and $M_{23} > 1000$ MeV, along with the integrated luminosities for E835 and E760. The figure shows the clustering of high-probability events near 3526 MeV.

(4) Figure 7 shows the M_{23} distribution, before and after (shaded) application of the cm angular cuts and the χ^2 probability cut, in which clear η and η' peaks are seen from $\pi^0\eta$ and $\pi^0\eta'$ events. We restrict the analysis to $M_{23} > 1000$ MeV, thereby reducing the acceptance to $\sim$3.2%. Here we use the measured rather than fitted M_{23}, since we are discriminating against background events with more than three photons, and the 3γ fit pulls the energies and momenta in those events to satisfy the kinematical constraints.

In the h_c search region there are 8 events for E835-1997 and 7 events for E835-2000. We plot M_{12} for these events in Fig. 8 with the corresponding distribution derived from the simulation. The distributions for both data sets are compatible with the simulation. The observed cross section for $\overline{p}p \to \eta_c\gamma$ is plotted in Fig. 9. We note that the background cross section is large near $\sqrt{s} = 3400$ MeV and decreases rapidly with energy.

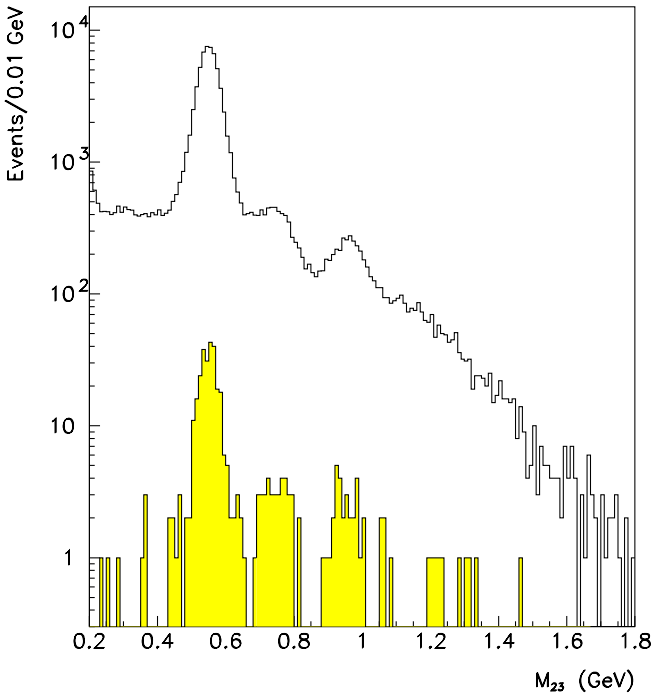

FIG. 7 (color online). The measured invariant mass M_{23}, showing η and η' peaks. A cut has been made that removes events containing π^0s. The shaded histogram represents events remaining after the cm angular cuts and an adequate fit to $\eta_c\gamma$. The final analysis is restricted to $M_{23} > 1000$ MeV.

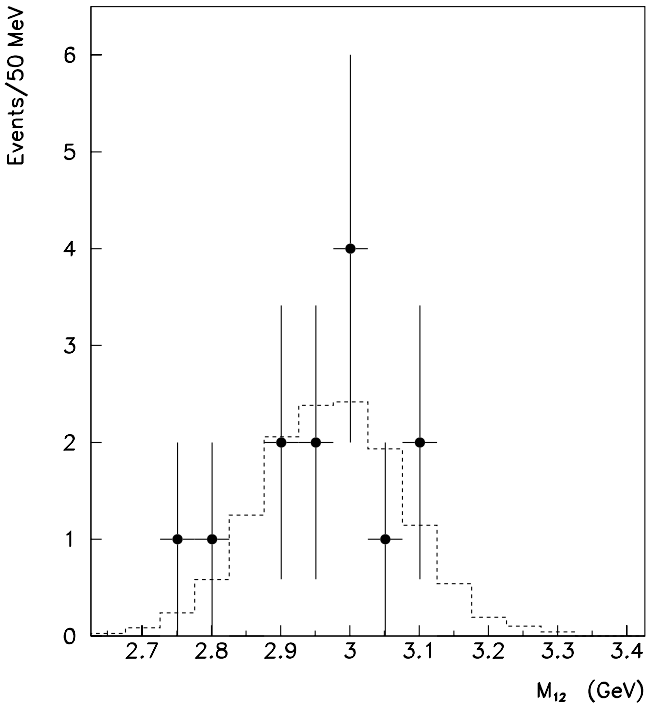

FIG. 8. The measured invariant mass of the two highest-energy photons for the h_c candidates between 3525.6 and 3526.4 MeV. The dashed histogram is the corresponding distribution obtained from the simulation. The rms widths for the data and simulation are compatible.

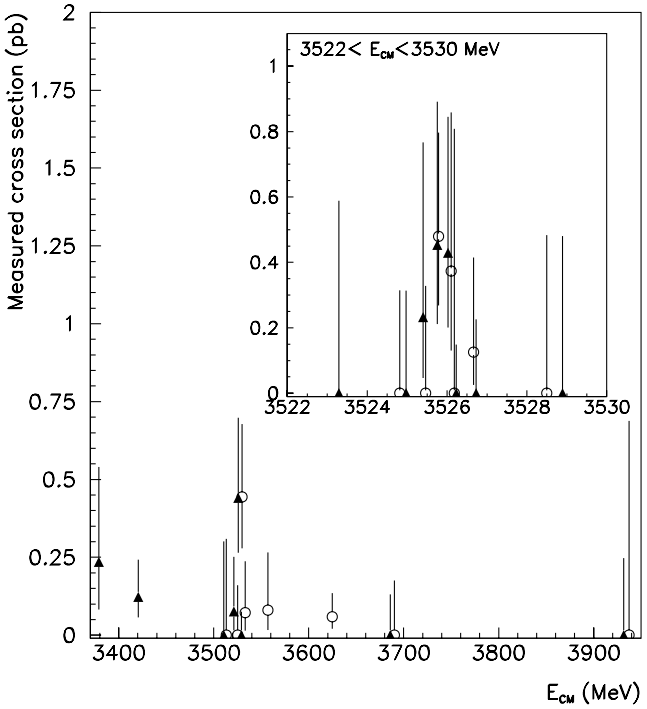

FIG. 9. The cross section for $\overline{p}p \to \eta_c\gamma \to \gamma\gamma\gamma$. The inset shows an expanded view of the h_c search region. The E835-1997 data are open circles and the E835-2000 data closed triangles.

We make the following tests: For events away from the h_c search region, we rescale the γ energies by the ratio $3526.2/\sqrt{s}$(MeV) and examine the resulting Dalitz plots for events appearing in the $\eta_c\gamma$ band. No candidates are present. We also examine the sensitivity of the selection to the value of m_{η_c} used in the 5C fit. Within the range $2850 < m_{\eta_c} < 3150$ MeV, the selection is unaffected.

2. Significance of the resonant signal

There are several methods for estimating the significance of the event excess in the $\eta_c\gamma$ channel.

(1) Binomial significance with *a priori* alternate hypothesis: We test the null hypothesis $H0$, that the cross section is the same in the signal bin and background bin, against the alternate resonant hypothesis $H1$, that the signal bin has a larger cross section, where the signal bin is chosen from the E760 $J/\psi\pi^0$ analysis. We bin the E760 data in the h_c search region ($3522.6 < \sqrt{s} < 3527.15$ MeV) so that the peak observed is contained in a single *signal* bin between 3525.6 and 3526.4 MeV. For the E835-1997 data, the integrated luminosity for the h_c signal bin is 19.07 pb^{-1}, and that for the background bin, extending from the χ_{c1} to χ_{c2} but excluding the signal bin, is 40.05 pb^{-1}, for binomial coefficient $P_b = 0.323$. There are 7 events in the signal bin and 2 in the background bin for $\mathcal{P} = 0.0068$. For the E835-2000 data, the corresponding values are 25.69 pb^{-1} in the signal bin and 31.73 pb^{-1} in the background bin for $P_b = 0.447$, and 6 events in the signal bin and 1 in the background bin, for $\mathcal{P} = 0.035$. Combining both data sets we have 44.76 pb^{-1} in the signal bin, 71.78 pb^{-1} in the background bin, $P_b = 0.384$ and $\mathcal{P} = 0.000\,59$. These results are summarized in Table III.

(2) Binomial significance with *a posteriori* alternate hypothesis with correction for multiple hypotheses: We select a bin with the expected width containing the event excess, test $H0$ against $H1$ as above, and multiply the resulting $\mathcal{P}$ by the number of independent $H1$ (Bonferroni correction). For a 0.5 MeV signal bin we find 12 events in $3525.7 < \sqrt{s} < 3526.2$ MeV with integrated luminosity 31.79 pb^{-1}, and 4 events in the remaining background bin between the χ_{c1} to χ_{c2} containing 84.75 pb^{-1} for $P_b = 0.273$. Taking the conservative Bonferroni factor 10 we find $\mathcal{P} = 0.0009$. For a 1.0 MeV signal bin we have 13 events in $3525.7 < \sqrt{s} < 3.5267$ MeV (49.85 pb^{-1}) and 3 events between the χ_{c1} and χ_{c2} (66.69 pb^{-1}) for $P_b = 0.428$ and, taking a Bonferroni factor 5, $\mathcal{P} = 0.010$. We note that if we impose a more restrictive cut, $M_{23}^2 > 1.2$ GeV^2, so as to exclude more events under the η' peak, then we are left with 8 events in the region $3525.4 < \sqrt{s} < 3526.2$ MeV, and 2 events outside the h_c signal region, for the combined data sets. This result, with reduced statistics, still corresponds to a very low binomial probability for the null hypothesis.

(3) Poisson significance: We estimate the expected number of background events n_b in a bin with the expected width, derived from a linear fit to the background cross section. Using our full data set, $3300 < \sqrt{s} < 4400$ MeV, we estimate the background cross section at 3526.2 MeV to be 79 ± 16 fb yielding $n_b = 2.51 \pm 0.51$ for $3525.7 < \sqrt{s} <$

TABLE III. Binomial $\mathcal{P}$s for the $\eta_c\gamma$ channel in E835-1997, E835-2000, and for both runs combined, using the *a priori* (E760) signal bin.

Run	L(signal) (pb^{-1})	L(back) (pb^{-1})	P_b	N(signal)	N(back)	$\mathcal{P}$
E835-1997	19.07	40.03	0.323	7	2	0.0068
E835-2000	25.69	35.03	0.447	6	1	0.035
E835-combined	44.76	75.06	0.384	13	3	0.000 59

3526.2 MeV ($n_b = 3.94 \pm 0.80$ in $3525.7 < \sqrt{s} < 3526.2$ MeV). The Poisson probability for ≥ 12 (≥ 13) events in the respective interval is 0.000 039 (0.000 63). We again take a Bonferroni factor 10 (5) and obtain $\mathcal{P} = 0.000\,39(0.0031)$.

(4) Significance from the likelihood ratio: As described below, we simulate 50 001 experiments with the conditions of E835 under the hypothesis of a linear background, and find the probability that a likelihood as large or larger as that observed arises by chance, yielding $\mathcal{P}$ between 1×10^{-3} and 3×10^{-3} depending upon the assumed resonance width.

We have tested the null hypothesis of a uniform cross section against the alternative hypothesis of a narrow peak in the expected h_c region. All of our tests yield a highly significant $\mathcal{P}$. In the absence of a narrow peaking background, these provide strong evidence for a resonance near 3526 MeV.

3. Resonance and background parameters

We fit the measured cross section to the sum of background and resonance terms, the latter Breit-Wigner with resonance energy E_R and width Γ_R, convolved with the density function of the cm energy, which is taken as Gaussian with rms width $\sigma_{\sqrt{s}}$ determined for each run. The data are binned by both $\sqrt{s}$ and $\sigma_{\sqrt{s}}$ so we can include the latter in the model, and fit by the Poisson maximum likelihood method. The expected number of events for the ith bin at mean cm energy $\sqrt{s} = E_i$, mean cm-energy rms width $\sigma_{\sqrt{s}} = \sigma_i$, bin width ΔE_i and integrated luminosity L_i, is

$$f_i(E_R, \Gamma_R, \sigma_p, \sigma_{bkgd}) = L_i \Big[\sigma_{bkgd}(E_i) + \frac{\sigma_p \Gamma_R^2/4}{(2\pi)^{1/2}\sigma_i} \times \int_{\Delta E_i} \frac{e^{-(E'-E_i)^2/2\sigma_i^2} dE'}{(E'-E_R)^2 + \Gamma_R^2/4} \Big], \quad (4)$$

where $\sigma_p = \epsilon_{\rm out} \frac{3\pi}{k^2} \mathcal{B}_{\bar{p}p} \mathcal{B}_{\eta_c\gamma}$, $\epsilon_{\rm out}$ is the acceptance $\times$ efficiency product, $k^2 = (E_R^2 - 4m_p^2)/4$, and $\sigma_{bkgd}(E)$ is parametrized as $\sigma_0 + b(E(\text{MeV}) - 3526.2)$. The data are insufficient to fit for Γ_R. This is not surprising as the putative resonance peak is narrow and evidently undersampled. For fixed values of Γ_R in the range 0.5–1.0 MeV, we obtain the values of E_R, σ_p, σ_0 and b that minimize the negative log likelihood:

$$-\ln\mathcal{L}(E_R, \sigma_p, \sigma_{bkgd}) = -\sum N_i \ln f_i + \sum f_i + \sum \ln N_i! \quad (5)$$

We fit the data from 3300 to 4400 MeV. The χ_{c_1} and χ_{c_2} data provide nearby background regions on either side of the h_c search region. The background is mainly due to $3\pi^0$ events where the π^0 decays are symmetrical or highly asymmetrical, thus simulating single photons. Background from $\eta\pi^0\pi^0$ events is reduced in comparison to $3\pi^0$ by the much smaller cross section, and by the smaller laboratory β of the η. Of 23 events selected, 15 are in the h_c region with the rest in the χ_{c_0}, χ_{c_2}, and η_c' search regions. The results are given in Table IV for five values of Γ_R. We observe that the background parameters are relatively independent of Γ_R, and that the signal strength $\Gamma_{\bar{p}p}\mathcal{B}_{\eta_c\gamma}$ increases slowly from 10.0 ± 3.5 to 12.0 ± 4.5 eV as Γ_R increases from 0.5 to 1.0 MeV. The maximum likelihood favors smaller Γ_R. $\mathcal{P}$ (nominal), a relative measure of significance obtained from the approximation that $-2\Delta\ln\mathcal{L}$ for the resonant less the nonresonant hypothesis is distributed as $\chi^2(1)$, is given in Table IV.

We also perform a Poisson maximum likelihood fit to the model of Eq. (4) where we add the expected angular dependence of the background and signal terms. The background angular distribution within the angular interval $-0.4 < \cos\theta_3^* < 0.7$ is obtained from events in the interval 3522 MeV $< \sqrt{s} <$ 3529 MeV satisfying all selection criteria except for the photon weight cuts and the χ^2 proba-

TABLE IV. Fits to the E835-1997 and E835-2000 $\eta_c\gamma$ data in the energy range $3300 < \sqrt{s} < 4400$ MeV. The background is linear with cross section σ_0 at 3526.2 MeV and slope b. The binning is: $\sqrt{s}$ by 150 keV, $\sigma_{\sqrt{s}}$ by 50 keV; $N_{\rm bins} = 64$. The nominal significance $\mathcal{P}$(nominal) is derived from the approximation that $-2\Delta\ln\mathcal{L}$ for the resonant vs the nonresonant hypothesis is distributed as $\chi^2(1)$. $\mathcal{P}$(sim) is determined by simulation, and is the probability that the likelihood ratio for the resonance-plus-background hypothesis vs the background-only hypothesis is greater than the experimental value. $\mathcal{P}(\text{sim})^\dagger$ is also determined by simulation and is the probability that both the likelihood ratio and the signal strength $\Gamma_{\bar{p}p}\mathcal{B}_{\eta_C\gamma}$ for the resonance-plus-background hypothesis vs the background-only hypothesis are greater than the experimental values.

Γ_R (MeV)	E_R (MeV)	$\Gamma_{\bar{p}p}\mathcal{B}_{\eta_c\gamma}$ (eV)	σ_0 (fb)	b (fb/MeV)	$-\log\mathcal{L}$	$\mathcal{P}$(nominal) ($\times 10^{-3}$)	$\mathcal{P}$(sim) ($\times 10^{-3}$)	$\mathcal{P}(\text{sim})^\dagger$ ($\times 10^{-3}$)
0.5(fixed)	$3525.83^{+0.15}_{-0.16}$	$10.0^{+3.8}_{-3.3}$	77^{+30}_{-24}	-0.36	34.19	0.30	0.98	0.86
0.7(fixed)	$3525.82^{+0.18}_{-0.19}$	$10.8^{+4.2}_{-3.6}$	79^{+31}_{-25}	-0.37	34.86	0.62	1.90	1.70
0.8(fixed)	$3525.82^{+0.19}_{-0.20}$	$11.2^{+4.4}_{-3.8}$	80^{+31}_{-25}	-0.37	35.15	0.85	2.28	2.08
0.9(fixed)	$3525.81^{+0.21}_{-0.22}$	$11.6^{+4.7}_{-4.0}$	80^{+32}_{-25}	-0.38	35.41	1.1	2.74	2.40
1.0(fixed)	$3525.81^{+0.22}_{-0.23}$	$12.0^{+4.9}_{-4.2}$	81^{+32}_{-25}	-0.38	35.66	1.5	3.16	2.76
No resonance:			156^{+35}_{-30}	-0.74	40.72			

bility cut for the $\eta_c\gamma$ fit. It is compatible with isotropy. The signal angular distribution is $\propto \sin^2\theta_3^*$. The fitted parameters do not significantly change but $\ln\mathcal{L}$ increases by 2.68 suggesting that the expected E1 decay angular distribution is a better hypothesis than isotropic decay.

The result for $\Gamma_{\overline{p}p}\mathcal{B}_{\eta_c\gamma}$ is consistent with the expected branching ratios of several $\times 10^{-5}$ for the $\overline{p}p$ mode and about 0.5 for the $\eta_c\gamma$ mode [7,9]. We numerically estimate the significance of the resonant signal by simulating 50 001 experiments using the background hypothesis, taking the integrated luminosity at each energy to be the experimental value, and fitting to background plus resonance hypothesis, allowing $3525.2 < M_R < 3527.2$ and fixing Γ_R between 0.5 and 1.0 MeV. We test the background hypothesis against the alternative hypothesis of background plus a resonance by computing the probability that a signal appears by chance that is at least as significant and/or as large as that observed experimentally. The numerical $\mathcal{P}$s, given in Table IV, fall between 1 and 3×10^{-3}, compatible with the significance found by binomial Poisson analysis.

B. $J/\psi\pi^0$ reaction

The detection of this decay channel is comparatively easy since the J/ψ provides a strong signature with small accidental background. However the study of the resonant channel is complicated by the presence of a continuum $\overline{p}p \to J/\psi\pi^0$ signal predicted by theory [10] and detected by E760 at the predicted level. Since continuum and possible resonant amplitudes would interfere, the energy dependence of the cross section could be asymmetrical. Further, detectability of a narrow resonance depends crucially on the width of the beam and on the integrated luminosity distribution.

1. Trigger and Event Selection

The trigger for the inclusive reaction,

$$\bar{p}p \to J/\psi + \text{anything} \to e^+e^- + \text{anything}, \qquad (6)$$

was designed to accept events with a large-mass e^+e^- pair within the acceptance of the central detector. It was implemented by requiring two charged tracks as defined by a coincidence between two hodoscope counters (H1 × H2) aligned in azimuth, with at least one of the two particles tagged as an electron by a signal in the corresponding Čerenkov cell. In addition, two large energy deposits (clusters), separated by more than 90° in azimuth and with an invariant mass greater than 60% of the center-of-mass energy, were required in the CCAL. The efficiency of this trigger was measured to be 0.90 ± 0.02 from a clean sample of $\bar{p}p \to \psi' \to e^+e^-$ events, taken with relaxed trigger conditions. On-line, a filtering program identified electron candidates as CCAL energy clusters aligned with tracks formed by the hodoscopes and Čerenkov elements.

Off-line, we require that the electron quality index EW exceeds 1.5. This quantity is a likelihood ratio based on scintillation counter and Čerenkov counter pulse heights, and CCAL cluster moments of both electron tracks. It is described in Ref. [3]. We limit the $e^+(e^-)$ acceptance to the Čerenkov fiducial region ($15° < \theta < 60°$), and require that the e^+e^- invariant mass exceeds 2800 MeV.

Of the events passing these cuts we only accept those compatible with

$$\bar{p}p \to J/\psi + \pi^0 \to e^- + e^+ + 2\gamma, \qquad (7)$$

restricting the acceptance of the two photon clusters to the CCAL fiducial region ($12° < \theta < 68°$) and their measured times to be within 10 ns of the event time derived from the trigger. Additional on-time CCAL clusters are allowed only if they are compatible with photons radiated by the e^+ or e^- ($E_{\text{clust}} < 100$ MeV and $\theta_{\gamma e} < 10°$). Finally, a six-constraint fit to reaction (7) is applied, and events with χ^2 probability less than 10^{-2} are rejected. With this set of cuts the selection efficiency is approximately 25% and the residual fraction of accidentals is estimated to be less than 10%.

2. Cross section

In Fig. 10 we plot the measured cross section for reaction (7) over the full center-of-mass energy range scanned

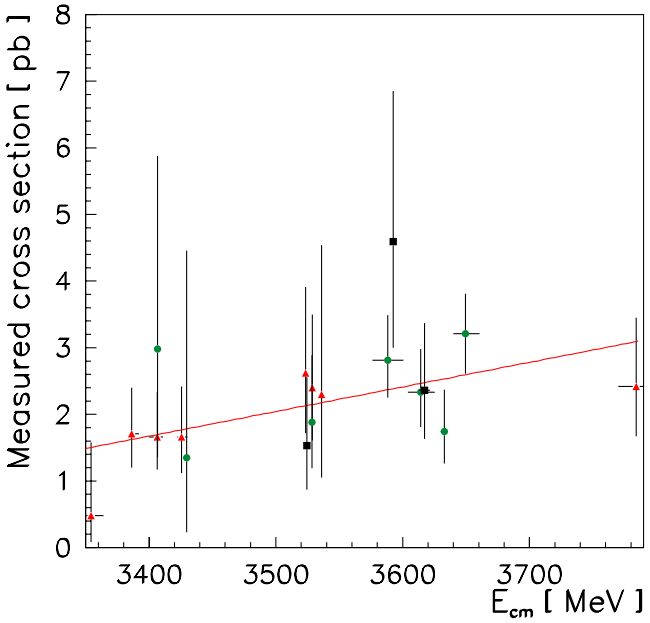

FIG. 10 (color online). Measured cross section for $\bar{p}p \to J/\psi + \pi^0 \to e^- + e^+ + 2\gamma$ over the full center-of-mass energy range scanned by E835. The E835-1997 data are circles and the E835-2000 data are triangles. The squares are the E760 measurements. Binning is done in 300 keV intervals. When the luminosity and number of events collected in a bin are small, adjacent bins are combined. The horizontal bars give the energy uncertainties obtained by in-quadrature summing of bin widths and beam spreads. We show a linear fit to the E835-1997 and E835-2000 data.

by E835, but excluding (a) the χ_1, χ_2, ψ' resonance regions to avoid background from J/ψ inclusive decay channels, and (b) the h_c search region ($3524 < \sqrt{s} < 3527$ MeV). The cross section increases slowly with energy and is compatible with that measured by E760 (black squares). The measured value at $\sqrt{s} = 3526$ MeV is $\sigma = 2.14 \pm 0.17$ pb.

In Fig. 11 we plot the cross section for reaction (7) observed in the h_c search region, compared to the continuum level determined from the data of Fig. 10, combining data from the 1996–1997 (circles) and the 2000 (triangles) running periods. For comparison purposes, we show an extrapolation of the E760 result to E835 data-taking conditions (squares). The E760 *data points* were obtained by selecting, from the published E760 sample, events fully contained in the CCAL (51 out of 67), to generate a sample compatible with the E835 data presented in this paper. The E760 event yields, bin by bin, were scaled by the ratio of the E835 to E760 integrated luminosities. (We note that removing events with photons in FCAL decreases the acceptance by ~0.75 and considerably reduces the significance of the E760 signal.) In the E835 data there is no evidence of an event excess that would correspond to a narrow (< 1 MeV) resonance.

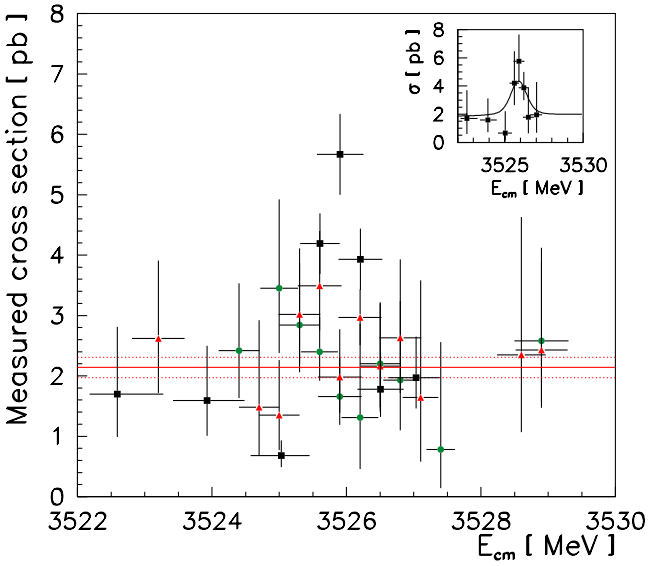

FIG. 11 (color online). Measured cross section for $\bar{p}p \to J/\psi + \pi^0 \to e^- + e^+ + 2\gamma$ within the h_c search region. The E835-1997 data are circles and the E835-2000 data are triangles. When the luminosity and number of events collected in a bin are small, adjacent bins are combined. The horizontal bars give the energy uncertainties obtained by in-quadrature summing of bin widths and beam spreads. The solid line and the $\pm 1\sigma$ dotted lines show the continuum level determined from the data of Fig. 10. The squares represent an extrapolation of the E760 data (shown in the inset with a superimposed fit to a Breit-Wigner function of 500 keV width) to E835 data-taking conditions, where the event yields are scaled up, bin by bin, by the ratio of E835 to E760 integrated luminosities and the resulting points plotted as squares.

3. Significance of the resonant signal

We estimate the significance of a possible event excess in the $J/\psi\pi^0$ channel in the same way as for the $\eta_c\gamma$ channel. We exclude the χ_{c1} and χ_{c2} resonance regions, since the radiative decays to $J/\psi\gamma$ constitute a background to $J/\psi\pi^0$, and consider only data for $3520 < \sqrt{s} < 3540$ MeV.

(1) Binomial significance with *a priori* H1: We test the null hypothesis H0 that the cross section is the same in the signal bin and background bin, taking the same *E760 signal bin* as above between 3525.6 and 3526.4 MeV, which for E835-1997 contains 19.07 pb^{-1}. The background bin contains 23.13 pb^{-1}, giving a binomial coefficient for the background hypothesis of $P_b = 0.45$. There are 40 events in the signal bin and 55 in the background bin for $\mathcal{P} = 0.76$. For E835-2000, the corresponding values are 25.69 pb^{-1} in the signal bin and 24.63 pb^{-1} in the background bin for $P_b = 0.51$, and 74 events in the signal bin and 56 in the background bin, for $\mathcal{P} = 0.11$. Combining both data sets we have 44.76 pb^{-1} in the signal bin, 47.76 pb^{-1} in the background bin, $P_b = 0.48$ and $\mathcal{P} = 0.27$. We also consider the bins containing the $\eta_c\gamma$ excess: (i) $3525.7 < \sqrt{s} < 3526.2$ MeV, $P_b = 0.344$, 68 signal events, 157 background events, $\mathcal{P} = 0.92$, (ii) $3525.7 < \sqrt{s} < 3526.7$ MeV, 116 signal events, 109 background events, $P_b = 0.54$, $\mathcal{P} = 0.78$.

(2) Binomial significance with *a posteriori* H1: There is no bin of 1 MeV or less in width that contains a substantial event excess.

(3) Poisson significance: Assuming a flat cross section for $3520 < \sqrt{s} < 3540$ MeV, and obtaining $\sigma_b = 2.4 \pm 0.24$ pb from the intervals $3520 < \sqrt{s} < 3525.6$ MeV and $3526.7 < \sqrt{s} < 3540$ MeV, we find $n_b = 76.29$ and 119.6 respectively for the 0.5 and 1.0 MeV intervals used in the $\eta_c\gamma$ analysis. The corresponding event totals are 68 and 116, fully compatible with the background hypothesis.

We have no significant enhancement in the $J/\psi\pi^0$channel and do not confirm the resonance reported by E760. The data are compatible with a flat cross section for $\sqrt{s}$ between 3520 and 3540 MeV. An independent analysis of these data [11] reached a similar conclusion.

III. CONCLUSION

We have measured the cross section for $\bar{p}p \to \eta_c\gamma$, $\eta_c \to \gamma\gamma$ in the vicinity of the center of gravity of the charmonium ^3P_J states and observe a narrow structure ($\Gamma \leq 1$ MeV) centered at $\sim 3525.8 \pm 0.2$ MeV. The statistical significance of the signal corresponds to a $\mathcal{P}$ value

of $\sim$0.001, where compatible values are obtained using binomial and Poisson counting analyses, and from the maximum likelihood method, where we simulate the expected distribution of likelihood ratio. The signal strength, given by $\Gamma_{\bar{p}p}\mathcal{B}_{\eta_c\gamma} \sim 12.0 \pm 4.5$ eV is compatible with the expected $\overline{p}p$ and $\eta_c\gamma$ branching ratios of the h_c. The signal is seen with equal strength and at the same M_R in the 1997 and 2000 runs of experiment E835. For the signal region integrated luminosity of $\sim$9 pb^{-1} taken in E760, we would have observed between 2 and 3 events in this channel. This observation is evidence for the h_c at its expected location near the center of gravity of the charmonium ^3P_J states.

We have measured the cross section for $\bar{p}p \rightarrow J/\psi\pi^0$ and observe no significant event excess in the χ_{cJ} center-of-gravity region.

ACKNOWLEDGMENTS

We gratefully acknowledge the support of the Fermilab staff and technicians and especially the Antiproton Source Department of the Beam Division and the On-Line Department of the Computing Division. We wish to thank also the INFN and University technicians and engineers from Ferrara, Genova, Torino and Northwestern for the valuable work done. This research has been supported by the Italian Istituto Nazionale di Fisica Nucleare (INFN) and the Department of Energy.

[1] N. Brambilla *et al.*, hep-ph/0412158.
[2] T. A. Armstrong *et al.*, Phys. Rev. Lett. **69**, 2337 (1992).
[3] G. Garzoglio *et al.*, Nucl. Instrum. Methods Phys. Res., Sect. A**519/3**, 558 (2004).
[4] E. Eichten *et al.*, Phys. Rev. D**17**, 3090 (1978), and references therein.
[5] D. B. Lichtenberg and R. Potting, Phys. Rev. D**46**, 2150 (1992), and references therein.
[6] S. Eidelman *et al.* (Particle Data Group), Phys. Lett. B **592**, 1 (2004).
[7] G. T. Bodwin, E. Braaten, and G. P. Lepage, Phys. Rev. D**51**, 1125 (1995).
[8] M. Andreotti *et al.*, "A Study of Two Neutral Pseudoscalar Mesons at the $\chi_{c0}(1^3P_0)$ Formation Energy" (unpublished).
[9] Y.-P. Kuang, S.-F. Tuan, and T.-M. Yan, Phys. Rev. D **37**, 1210 (1988).
[10] M. K. Gaillard, L. Maiani, and R. Petronzio, Phys. Lett. B **110**, 489 (1982).
[11] D. Joffe, Ph.D. dissertation, Northwestern University, 2004 (unpublished).